Reconfigurability of graphene-based hexagonal patch operating in the Ku band

Hassna Agoumi[1], Seddik Bri[2], Youssef El Amraoui[3], Adil Saadi[1]
[1]Modeling, Information Processing and Control Systems (MIPCS), National Graduate School of Arts and Crafts, Moulay Ismail University, Meknes, Morocco
[2]Intelligent Electrical Systems, Materials and Components, High School of Technology, Moulay Ismail University, Meknes, Morocco
[3]Laboratory of Condensed Matter and Indisciplinary Science (LaMCScI), Faculty of Science, Mohammed V University, Rabat, Morocco

Article Info

Article history:

Received Dec 18, 2025
Revised Apr 14, 2026
Accepted May 25, 2026

Keywords:

Frequency tuning
Graphene-based antenna
Hexagonal patch antenna
Impedance reconfigurability
Ku-band antenna
Planar antenna array
Surface conductivity control

ABSTRACT

This paper presents a novel graphene-based impedance reconfigurability approach for Ku-band hexagonal patch antennas, demonstrated at both the single-element and 4×4 array levels. Unlike conventional metallic or diode-based reconfigurable antennas, frequency tuning is achieved by exploiting the tunable surface conductivity of graphene integrated into E-shaped slots, without altering the antenna geometry or employing active lumped components. Antenna performance is evaluated using full-wave electromagnetic simulations for two graphene states ("on" state and "off" state), representing distinct surface impedance conditions. The single element exhibits dual resonances at 14.81 GHz and 15 GHz, with reflection coefficients of -52.56 dB and -38.18 dB, bandwidths of 783 MHz and 517 MHz, and a peak gain of 7.8 dBi. The 4×4 array exhibits multiple resonances between 12.5–16.8 GHz (off state) and 12.6–17.15 GHz (on state), achieving bandwidths up to 2750 MHz and a maximum gain of 13.64 dBi. These results demonstrate a scalable, geometry-preserving reconfigurable antenna solution for compact Ku-band systems.

Corresponding Author:

Hassna Agoumi
Modeling, Information Processing and Control Systems (MIPCS)
National Graduate School of Arts and Crafts, Moulay Ismail University
15290 ENSAM, Meknes 50500, Morocco
Email: h.agoumi@edu.umi.ac.ma

1. INTRODUCTION

Modern wireless applications, such as satellite communications, vehicular networks, and 5G/6G systems, are largely based on the exploitation of the Ku-band (12-18 GHz) [1]. Addressing the increasing demands for data rate, these applications require compact antenna systems with high gain, wide bandwidth, and stable radiation [2]. Recently, notable research focus has been allocated to the development of high-performance planar antennas operating in the Ku-band.

Although the radiation efficiency of conventional metal antennas is significant, their electromagnetic properties remain intrinsically static, due to the constant surface impedance of their metal radiators. Limited frequency tunability and a reduced adaptability to dynamic communication environments are thus the consequences of these antennas [3]. Although reconfigurable antennas based on positive intrinsic negative (PIN) diodes or varactors have been proposed, these approaches often introduce additional biasing complexity, ohmic losses, and potential degradation of radiation performance [4].

Several studies have advanced Ku-band antenna architectures using shared-aperture and fabry–perot cavity (FPC) concepts. A wideband dual-frequency shared-aperture antenna was demonstrated in [5], while polarization-reconfigurable FPC mechanisms were analyzed in [6]. For internet of things/vehicles (IoT/IoV) systems, a dual-band dual circularly polarized multibeam antenna was introduced in [7]. Frequency range or FR1/FR2 shared-aperture configurations in [8] and a switchable fan-beam module in [9] were also proposed. Further innovations include a dual-band reflective surface [10], a triple-band FPC and microstrip grid array [11], with gains >12.5 dBi, and a high-gain Ku-band phased array [12], achieving 32.4 dBi gain and 36.7 dB isolation. An S/K/Ka triple-band hybrid antenna was reported in [13] with beam scanning up to ±27°, and a compact dual-band circularly polarized navigation with Indian constellation (NavIC) antenna was presented in [14] with isolation >20 dB. Despite these advances, compact dual-band antennas with high isolation for emerging 6G IoV applications remain underexplored, motivating the present work.

In parallel, graphene has emerged as a promising material for next-generation electromagnetic devices due to its high carrier mobility and electrically tunable surface conductivity [15]. These properties enable compact and frequency-reconfigurable antenna structures, particularly at millimeter-wave and terahertz frequencies [16]. However, the integration of graphene-based tunable impedance into Ku-band patch antenna architectures remains largely unexplored. The dependence on conventional metal radiators with an intrinsically fixed surface impedance leads to limited adaptability of bandwidth and constrained dynamic frequency control in most Ku-band antennas. Although several reconfigurable antennas employ PIN diodes or varactors, these solutions introduce additional biasing complexity, ohmic losses, and potential degradation of radiation performance. Consequently, the realization of geometry-preserving Ku-band antenna arrays capable of intrinsic electromagnetic reconfigurability using tunable materials such as graphene remains an open research challenge.

Graphene is exploited in this work to propose a Ku-band reconfigurable antenna architecture, thus overcoming the limitations of conventional metal antennas. This paper makes the following contributions. First, a hexagonal microstrip patch antenna integrating graphene-filled E-shaped slots is proposed to achieve geometry-preserving impedance-controlled frequency reconfigurability. Second, a graphene-based electromagnetic tuning mechanism is implemented by exploiting the electrically tunable surface conductivity of graphene, enabling intrinsic frequency reconfigurability without the use of discrete switching components such as PIN diodes or varactors. Third, the proposed concept is systematically validated at two design scales, including a single radiating element and a 4×4 planar array configuration, demonstrating scalable reconfigurable behavior with stable gain characteristics and extended impedance bandwidth within the Ku-band. These results highlight the potential of graphene-based impedance modulation for the development of compact and adaptive Ku-band antenna systems.

The obtained results demonstrate effective frequency reconfigurability, stable gain characteristics, and bandwidth enhancement within the Ku-band. These findings highlight the potential of graphene-enabled antenna architectures for adaptive satellite and vehicular communication systems and provide a promising pathway toward the development of reconfigurable antennas for future 5G and 6G wireless networks.

2. METHOD

Based on four sequential steps, the proposed methodology includes the design of the hexagonal unit cell, the modeling of the graphene surface impedance, the construction of the 4×4 planar network; and the full-wave electromagnetic validation. The overall design and simulation workflow of the proposed antenna is illustrated in Figure 1.

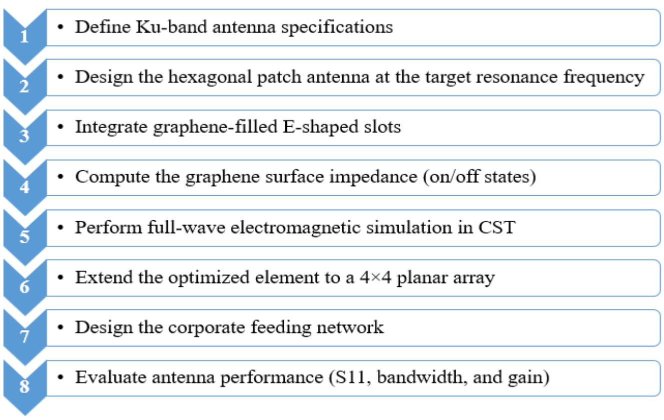

Figure 1. Flowchart of the proposed graphene-based antenna design and simulation procedure

2.1. Single hexagonal patch antenna

The radiating element is derived from the classical circular microstrip patch model operating in the Ku-band (12–18 GHz). The effective radius is calculated using the cavity model as in (1) [17]:

$$R_{eff} = \frac{c}{2f_r\sqrt{\varepsilon_{eff}}} \quad (1)$$

where R_{eff} denotes the effective patch radius (m), c is the speed of light in free space $(m \cdot s^{-1})$, f_r represents the target resonance frequency (Hz), and ε_{eff} is the effective dielectric constant of the substrate. The essential parameters of the proposed antenna are summarized in Table 1.

Table 1. Essential parameters of the proposed antenna

Parameter	Value
Resonant frequency (f_r)	14.64 GHz
Relative permittivity of the substrate (ε_r)	4.3
Thickness of the substrate (h)	1.6
Antenna input impedance R_{in}	50Ω

The circular geometry is transformed into a regular hexagonal patch while preserving the radiating area. The antenna is implemented on an FR4 substrate with relative permittivity $\varepsilon_r = 4.3$ and a thickness of 1.6 mm, and is excited through a 50 Ω microstrip feed line. The two graphene-filled E-shaped slots are inserted into the radiating patch to enable conductivity-controlled frequency tuning. The geometric parameters of the patch, slots, feed line, and ground plane are optimized to ensure proper impedance matching within the Ku-band. The geometry and design evolution of the proposed single-antenna element are illustrated in Figure 2. The initial regular hexagonal patch is presented in Figure 2(a), whereas Figure 2(b) shows the configuration incorporating two graphene-filled E-shaped slots. The optimized geometric dimensions are summarized in Table 2.

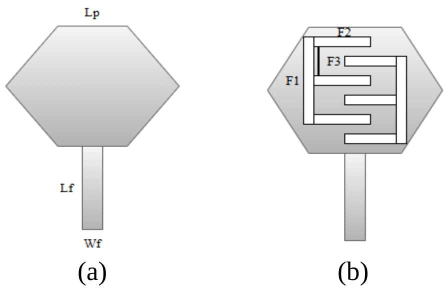

Figure 2. Geometry and design evolution of the proposed hexagonal patch antenna: (a) initial regular hexagonal configuration and (b) hexagonal patch incorporating graphene-filled E-shaped slots

Table 2. Optimized geometric dimensions of the proposed antenna

Parameter	Optimized value (mm)
Lp	7.94
Lf	7.97
Wf	3.28
$F1$	9.66
$F2$	6.30
$F3$	4.23

2.2. Graphene surface impedance modeling

Graphene strips integrated into the radiating patch act as tunable conductive elements that modify the surface current distribution. The tuning of the resonant frequency is achieved by altering the effective electrical length of the patch by variation of the surface impedance of the graphene. The two states of conductivity are thus analyzed: a low surface impedance characterizes the "on" state, favoring the conduction of current through the graphene strips, while a high surface impedance corresponds to the "off" state, limiting the circulation of current.

In order to analyze the intrinsic electromagnetic reconfigurability, a uniform polarization is adopted, where the same voltage V_g is applied to all graphene strips. The surface impedance is thus controlled by this direct-current (DC) bias voltage, which acts on the carrier density and the chemical potential μ_c. The graphene surface impedance is evaluated at the target resonance frequency within the Ku-band to ensure consistency with the antenna operating conditions. To determine practical values of the "on" and "off" surface impedances $Z_{s\,on}$, and $Z_{s\,off}$, the following (2)-(7) are used [18]:

$$\eta = \frac{\varepsilon_0 \varepsilon_r V_g}{dq} \tag{2}$$

$$\mu_c = \hbar v_f \sqrt{\eta\pi} \tag{3}$$

$$\tau_s = \frac{4\hbar^2 \rho_m v_f {V_{ph}}^2}{\sqrt{\eta\pi}\, K_B T D^2} \tag{4}$$

$$\tau_L = \frac{\mu_L \hbar \sqrt{\eta\pi}}{q v_f} \tag{5}$$

$$\frac{1}{\tau} = \frac{1}{\tau_L} + \frac{1}{\tau_s} \tag{6}$$

$$Z_s = \frac{1}{\sigma(f, \mu_c, \tau, T)} = \frac{j\pi\hbar^2 (2\pi f(\tau_L \tau_s) - j(\tau_L + \tau_s))}{q^2 (\tau_L \tau_s)\left[\mu_c + 2K_B T ln\left(e^{\frac{-\mu_c}{K_B T}} + 1\right)\right]} \tag{7}$$

Where η is the carrier density (m^{-2}), ε_0 is the vacuum permittivity ($F.m^{-1}$), ε_r is the relative permittivity of the dielectric layer, V_g is the applied gate bias voltage (V), d is the graphene thickness (m), and q is the elementary electron charge (C). In addition, μ_c denotes the graphene chemical potential (eV), $\hbar$ is the reduced Planck constant ($J.s$), and v_f is the Fermi velocity in graphene (m^{-1}). The parameters τ_s and τ_L represent the phonon-scattering and impurity-scattering relaxation times, respectively (s). Furthermore, $\rho_m = 7.6 \times 10^{-7}\ Kg/m^2$ is the two-dimensional mass density of graphene, $v_{ph} = 2.1 \times 10^4\ m/s$ is the velocity of longitudinal acoustic phonons, k_B is the Boltzmann constant ($J.k^{-1}$), T is the absolute temperature (K), D is the deformation potential (eV), and μ_L is the carrier mobility ($m^2.V^{-1}.S^{-1}$), Finally, Z_s represents the graphene sheet impedance ($\Omega/\square$) obtained from the complex surface conductivity $\sigma(f, \mu_c, \tau, T)$, where f is the operating frequency (Hz).

The selected parameter values used to compute $Z_{s\,on}$ and $Z_{s\,off}$ are summarized in Table 3. The applied gate bias voltage V_g modulates the carrier concentration in the graphene layer, which in turn modifies the chemical potential μ_c and the resulting surface conductivity. The "on" state corresponds to a higher carrier density and therefore a lower surface impedance, while the "off" state is associated with reduced carrier density and significantly higher surface impedance. In the electromagnetic simulations, graphene strips are implemented in CST Microwave Studio as frequency-dependent sheet impedances using the calculated complex surface impedance values. This approach allows controlled resonance tuning without introducing discrete radio frequency (RF) switching components.

Table 3. Selected parameters of the graphene surface impedance for "on" and "off" states

State	"on" state	"off" state
Gate-voltage V_g (V)	21	0.05
Temperature T (k)	300	300
Carrier concentration η (m^{-2})	5.8×10^{17}	6×10^{14}
Graphene surface impedance Zs(Ω/□)	6.09 + j0.5	1552 + j1.8

2.3. 4×4 hexagonal patch antenna array

An inter-element spacing of approximately 1.2 λ is adopted to balance reduction of the mutual coupling and the elimination of the grating lobes in the Ku-band. The optimized unit cell is then scaled into a 4×4 planar array configuration, leading to improved radiation performance in accordance with established array synthesis principles [19]. A corporate feed network is adopted to provide uniform amplitude and phase excitation across the array. The feeding structure employs quarter-wave impedance transformers with 50 Ω input matching and intermediate 70 Ω and 100 Ω transmission-line sections to ensure efficient power distribution, as commonly implemented in planar array feeding networks [20]. The λ/4 power divider transformer is shown in Figure 3.

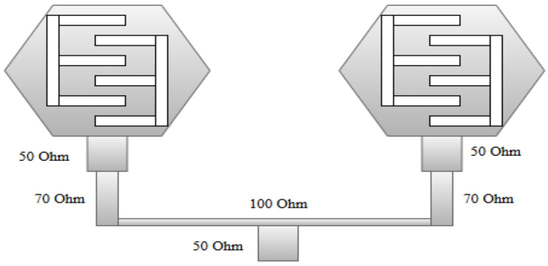

Figure 3. Power divider λ/4 transformer

The 4×4 planar array is formed by integrating the optimized unit cell within a symmetric corporate-fed topology to maintain coherent excitation across all elements. As shown in Figure 4, the full array structure is based on phase uniformity, which essential to ensure constructive interference in the main radiation direction and reduced sidelobe levels. All electromagnetic simulations are performed using the time-domain solver of CST Microwave Studio. The antenna is excited via a 50 Ω waveguide port, and open (radiation) boundary conditions are applied to emulate free-space propagation. An adaptive mesh refinement strategy is employed to ensure numerical convergence. In order to verify the numerical stability, additional simulations using different mesh densities have been carried out, showing gain variations of less than 0.3 dBi and deviations of $S11$ within ±0.8 dB. The performance of the antenna is then evaluated in terms of reflection coefficient ($S11$), impedance bandwidth, realized gain and radiation diagrams.

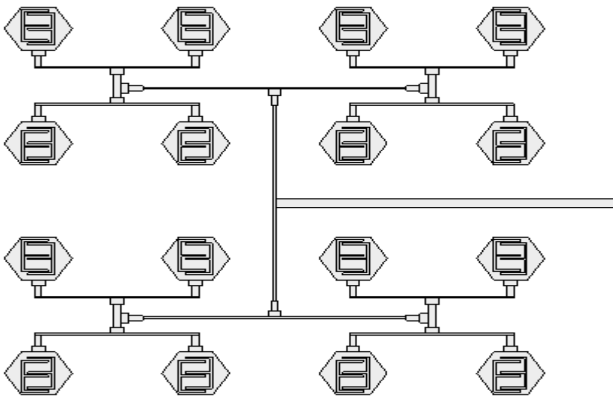

Figure 4. 4×4 hexagonal patch antenna array with corporate feeding network

3. RESULTS AND DISCUSSION

3.1. Single hexagonal patch antenna

As illustrated in Figure 5, the gate bias voltage V_g controls resonance by modulating both the carrier concentration η and graphene's surface impedance Z_s. In the "off" state, the higher sheet impedance restricts current flow, resulting in resonances at 13.72 GHz and 14.81 GHz. Increasing V_g to the "on" state lowers this impedance, allowing the current to distribute more freely along the slots. This shift moves the resonances to 13.75 GHz and 15.00 GHz. While the "off" state provides a broader bandwidth, the "on" state enhances conduction, ultimately achieving a tuning step of approximately 180 MHz. Advantageous for Ku-band reconfigurable systems, this capability enables dynamic frequency adaptation without geometric modification, owing to the tuning of graphene surface impedance, as validated by the variation of the reflection coefficient S11 under biasing conditions, while maintaining satisfactory impedance matching.

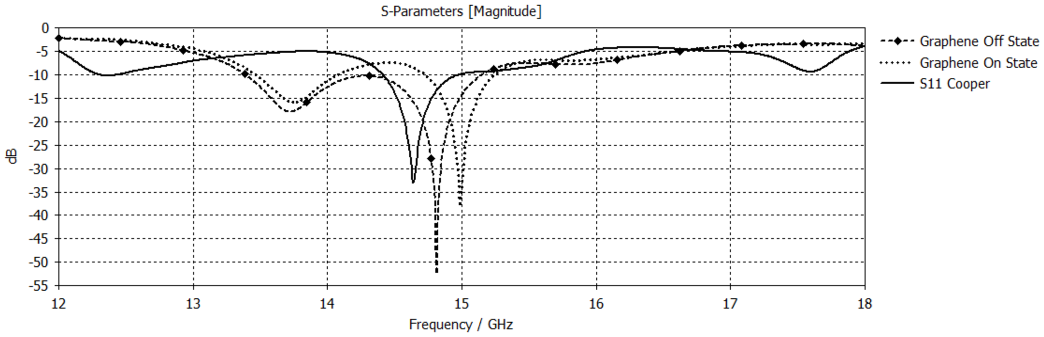

Figure 5. Simulated S11 response of the proposed antenna for graphene “off” / “on” states and copper

A slight degradation in impedance matching is observed due to the reduced conductivity of graphene, which alters the input impedance compared to the copper structure. This difference arises from ohmic losses induced by the higher surface impedance of graphene, which disrupts the current distribution on the radiating patch, unlike copper which supports nearly ideal conduction. Consequently, differences in resonance behavior and bandwidth are observed between the copper reference antenna and the graphene-based configuration, the latter being characterized by additional dissipative losses associated with its finite surface conductivity.

As shown in Figure 6, the gain peak shifts are governed by the bias control; the gain variation follows the resonance behavior previously discussed. In the “off” state, the higher sheet impedance restricts surface current propagation, increases dissipative losses, and shifts the maximum gain toward a lower frequency (14.7 GHz) with a reduced peak value (6.9 dBi). In the “on” state, the lower impedance facilitates current flow along the patch, improves radiation efficiency, and moves the gain maximum toward 15 GHz, where the peak reaches 7.8 dBi. Compared with the copper reference (8.7 dBi at 15 GHz), the graphene states exhibit a gain reduction of about 0.9 dBi (on) and 1.8 dBi (off), which quantifies the additional losses introduced by the finite conductivity of graphene.

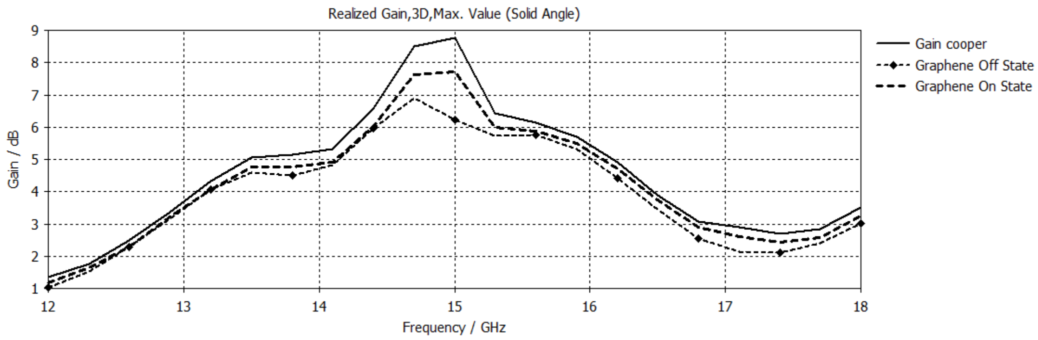

Figure 6. Realized gain response of the proposed antenna for copper and graphene “off” / “on” states

Adaptive radiation control and beam scanning are now feasible. For this purpose, planar antenna arrays are employed. The proposed unit element can act as a robust fundamental building block. Its radiation performance is consistent. This reflects its dependability. Despite the limited conductivity of graphene, the radiation efficiency stays satisfactory. The simulation results confirm this. The graphene-based tuning thus maintains this efficiency.

Figure 7 compares the far-field directivity patterns of the copper reference antenna and the graphene-based configurations. The copper as in Figure 7(a) patch exhibits a directivity of 7.37 dBi with a beam pointing direction of 48° and a -3 dB beamwidth of 65.5°. When graphene is introduced, the bias-controlled variation of the graphene surface impedance modifies the surface current distribution on the radiating patch. In the “on” state in Figure 7(b), the reduced sheet impedance enhances current propagation, yielding a directivity of 9.23 dBi with a narrower beamwidth of 41.4°. In the “off” state in Figure 7(c), the higher impedance partially restricts current flow, resulting in a broader beam with a -3 dB beamwidth of 73.7° and a directivity of 5.66 dBi.

The reduced realized gain observed in the “off” state is attributed to increased dissipative losses associated with the higher surface impedance of graphene, which also leads to a decrease in directivity. More generally, compared to copper, graphene-based configurations exhibit modified radiation characteristics due to the finite conductivity of graphene, which disrupts the current distribution and introduces additional losses. The ability to adjust radiation characteristics without modifying the antenna geometry is particularly attractive for frequency-agile and beam-steerable Ku-band communication systems, enabling adaptive control of radiation in reconfigurable antennas through bias-controlled operation.

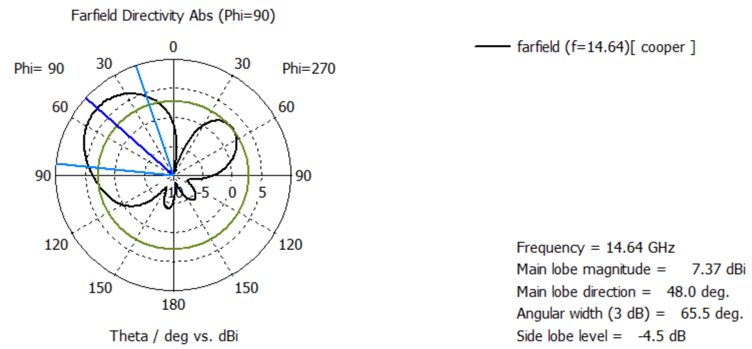

(a)

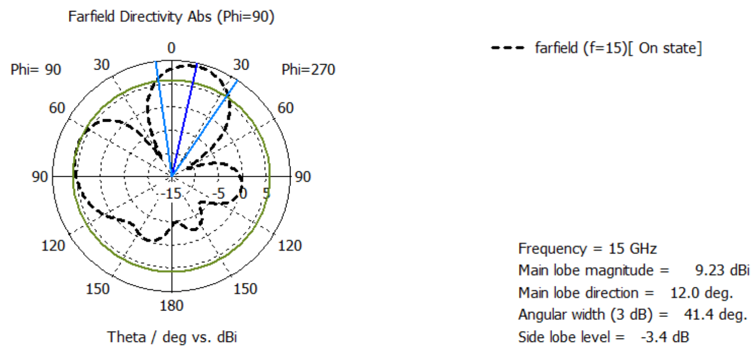

(b)

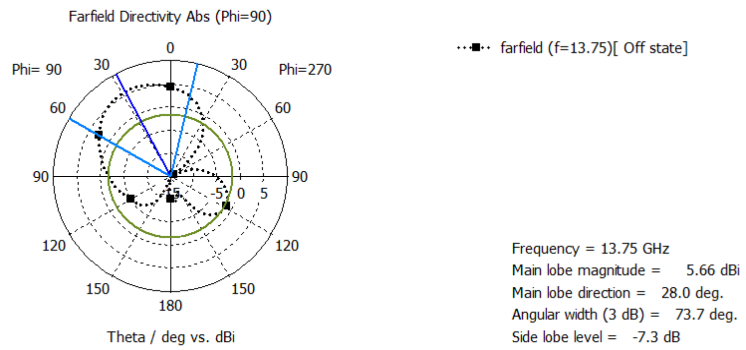

(c)

Figure 7. Radiation patterns of the single hexagonal patch antenna: (a) copper, (b) graphene “on”, and (c) graphene “off”

3.2. Feeding network characterization

The input reflection coefficient of the feeding network is presented in Figure 8. A strong resonance is obtained around the operating frequency, where S11 is below -20 dB. This confirms proper impedance matching when all output ports are terminated with 50 Ω loads. Minor secondary resonances are attributed to the multi-branch structure.

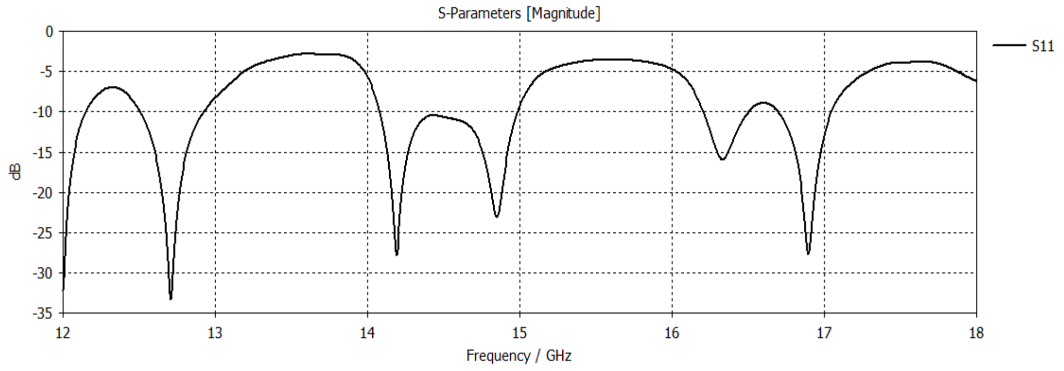

Figure 8. Reflection coefficient S11 of the feeding network with matched loads at all output ports

Figure 9 illustrates the transmission coefficients for representative ports (S21, S61, and S161). The curves exhibit similar behavior across the frequency band, confirming uniform power distribution. The insertion loss remains consistent among the outputs, validating the balanced nature of the network. These results demonstrate efficient power division.

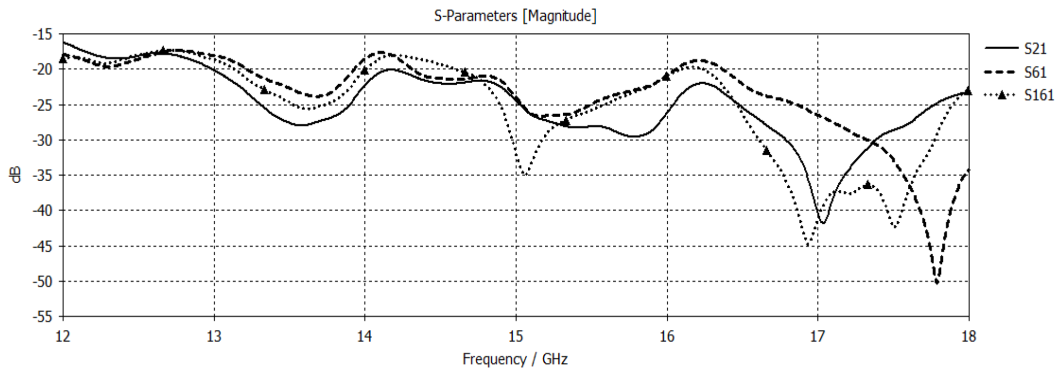

Figure 9. Insertion loss of the feeding network for representative output ports (S21, S61, and S161)

Figure 10 illustrates the isolation between representative output ports. An effective attenuation of the mutual coupling is translated by the fact that the majority of the coupling levels are maintained below -20 dB over the entire operating band. Reaching less than -30 dB, some pairs of ports have even lower values, which confirms the robustness of the power feeding network in minimizing interference. Since all the output ports have similar responses, only representative parameters S are considered, due to the symmetrical architecture of the power feeding network.

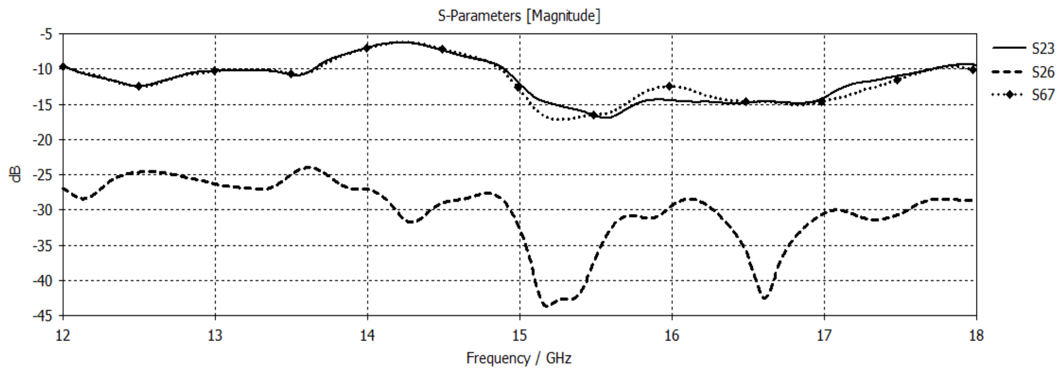

Figure 10. Isolation characteristics between representative output ports (S23, S26, and S67)

3.3. Hexagonal patch antenna array

Figure 11 presents the simulated reflection coefficient of the 4×4 array for the graphene "off" and "on" states. Multiple resonances appear across the Ku-band due to the interaction between the corporate feeding network and the mutual coupling among the radiating elements. In the "off" state, resonances occur at 12.5, 12.8, 14.1, 14.8, 16.3, and 16.8 GHz, with reflection minima ranging from -19 to -46 dB. When the graphene layer is biased ("on" state), the resonances shift to 12.6, 12.9, 14.4, 15.06, 16.5, and 17.15 GHz, corresponding to an average tuning of approximately 280 MHz.

This frequency shift originates from the bias-dependent variation of the graphene sheet impedance, which modifies the input impedance of the array through changes in inter-element coupling and feeding-network matching. This bias-controlled impedance modulation enables effective frequency tuning at the array level without modifying the antenna geometry. Such reconfigurable spectral behavior is beneficial for frequency-agile Ku-band antenna arrays used in adaptive communication systems. In addition, the stable multiresonant response provides a suitable foundation for scalable array architectures supporting dynamic beam control.

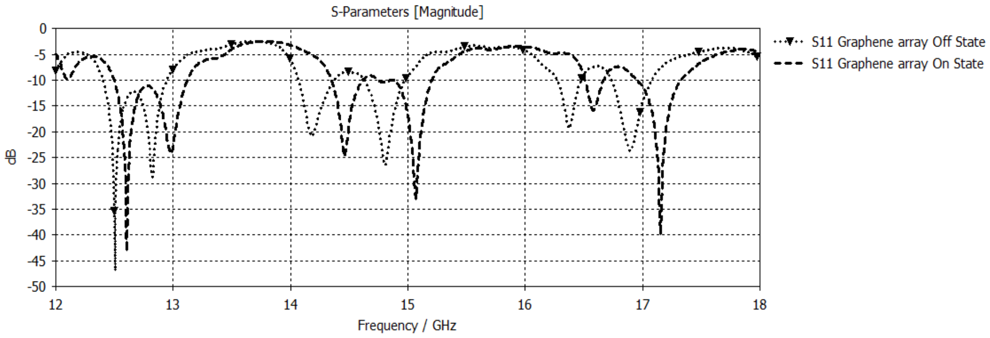

Figure 11. Simulated S_{11} of the proposed 4×4 graphene array for "off" and "on" states

Figure 12 presents the realized gain of the proposed 4×4 array for the graphene "off" and "on" states. The maximum gain occurs around 12.6 GHz, reaching 13.30 dBi in the "off" state and 13.64 dBi in the "on" state. The slightly higher gain in the "on" state results from the reduced graphene sheet impedance, which improves current conduction along the array elements and enhances radiation efficiency. In contrast, the "off" state exhibits stronger gain fluctuations due to the higher surface resistance associated with the reduced graphene conductivity.

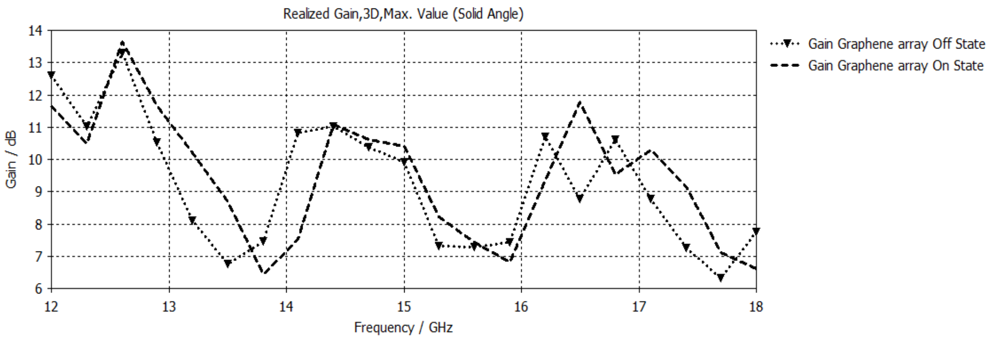

Figure 12. Simulated gain of the proposed 4×4 graphene array for "off" and "on" states

With a gain of up to 13.3 dBi, the 4×4 network confirms the efficiency of the corporate power feeding network. The modulation of the graphene impedance allows dynamic gain control and adaptive adjustment of the radiated power. The multiple peaks on the Ku band thus reveal a strong frequency selectivity and a reinforced high gain beamforming.

The proposed antenna design is compatible with standard fabrication processes. Graphene layers can be synthesized via chemical vapor deposition (CVD), transferred onto dielectric substrates, and patterned using conventional lithographic techniques for RF applications [21]. Fabrication tolerances may introduce dimensional deviations, leading to resonance shifts, impedance mismatch, and gain degradation. In addition, the electromagnetic performance of graphene is strongly influenced by its surface conductivity, which depends on material quality, transfer-induced defects, and contact resistance variability [22]. Future work will focus on prototype fabrication and experimental validation to address these factors and reduce uncertainty in practical implementations.

3.4. Comparaison with previous studies
3.4.1. Single hexagonal patch antenna

The proposed antenna is particularly suitable for Ku-band applications, especially on unmanned aerial vehicle (UAV) and satellite platforms, where compactness, reliability, and low complexity are essential requirements. Without relying on active components or complex polarization networks, it enables competitive gain while improving robustness to vibrations and thermal variations, as shown in Table 4. The continuous tunability further enables adaptive frequency operation in dynamic environments.

Table 4. Comparison of the proposed single hexagonal patch antenna with previously reported designs

References	Technology	GHz	MHz	dBi	Reconfigurability	Complexity
[23]	Circular patch + PIN diode (RT5880)	12.85 12.50	650 500	6.15 5.8	Yes	High (isolation circuits required, complex biasing networkDC, multiple PIN diodes)
[24]	Reuleaux monopole + DGS + 2 PIN diodes	13.7	2950	3.85	Yes	Medium (biasing lines affect radiation, defected ground structure, 2 PIN diodes)
[25]	Dual patch + LC phase shifters + couplers	12.00	1000	5.2	Yes	High (5-layer stack-up, 2 meandered phase shifters, DC decoupling structures, complex biasing)
This work	Hexagonal antenna with graphene E slots	14.81 15	783 517	6.9 7.8	Yes	Low (no active diodes, simple DC biasing through graphene, no complex isolation circuits)

3.4.2. Hexagonal patch antenna array

A competitive bandwidth of 2750 MHz and a gain of 13.64 dBi are demonstrated by the proposed 4×4 graphene-based antenna array, whose performance is benchmarked in the comparative overview of Table 5 against recently reported planar antenna arrays. Real-world constraints such as temperature stability, polarization integration and environmental robustness need to be evaluated for practical deployment in SATCOM, UAV, or 6G scenarios. These aspects will be addressed during future experimental validations.

Table 5. Comparison of the proposed 4x4 hexagonal patch antenna array with previously reported designs

References	Technology	GHz	MHz	dBi	Number of elements
[26]	2×4 circular patch array RT5880	12.33	310	7.6	8
[27]	FR4, circular monopoles, staircase isolation, unconnected ground, high-isolation multiple-input multiple-output (MIMO)	12	9530	11.57	4
[28]	Modified Koch fractal, coplanar waveguide (CPW) feed, meander line isolation, FR4, single-sided	14.39	1115	6.1	2
[29]	L-probe square-ring (LB), stacked patch (HB), multilayer printed circuit board (PCB) TLE-95/RO4450T, grounded CPW (GCPW) feed, Ku-band satellite communications (SATCOM)	13.21 15.32	2110	5.42	2
[30]	FR4, rectangular radiator, curved edges, partial ground slot, meandered band-notch, orthogonal elements	12	1000	4	4
This work	4×4 hexagonal antenna with graphene E slots	12.5, 12.8, 14.1, 14.8, 16.3, 16.8 (“off”) 12.6, 12.9, 14.4, 15.06, 16.5,17.15(“on”)	2480 (“off”) 2750 (“on”)	13.30 (“off”) 13.64 (“on”)	16

4. CONCLUSION

The potential of graphene as an active material for frequency-reconfigurable Ku-band antennas is highlighted in this study. Two resonant modes at 14.81 GHz and 15 GHz, with bandwidths of 783 MHz and 517 MHz and a peak gain of 7.8 dBi, are achieved by the proposed hexagonal patch. When extended to a 4×4 configuration, the antenna operates over 12.5–16.8 GHz (“off” state) and 12.6–17.15 GHz (“on” state), achieving a bandwidth of up to 2750 MHz, a peak gain of 13.64 dBi, reduced sidelobe levels, and stable impedance behavior. Although the results are obtained from full-wave simulations, experimental validation remains necessary for practical deployment. Future work will therefore focus on prototype fabrication and the integration of an appropriate graphene biasing network. Particular attention will also be given to system-level constraints such as weight, compactness, and electromagnetic compatibility when integrating the antenna into UAV or satellite platforms. In addition, alternative tunable materials and modified antenna configurations will be investigated to extend the proposed concept toward other frequency bands and applications. These developments position graphene-enabled antenna arrays as promising candidates for adaptive Ku-band satellite platforms and next-generation 6G communication systems.

ACKNOWLEDGMENTS

The authors would like to thank their institution for providing the facilities necessary to conduct this research. This work was carried out without any research grant or contract.

FUNDING INFORMATION

The authors declare that no funding was received for this work.

AUTHOR CONTRIBUTIONS STATEMENT

This journal uses the Contributor Roles Taxonomy (CRediT) to recognize individual author contributions, reduce authorship disputes, and facilitate collaboration.

Name of Author	C	M	So	Va	Fo	I	R	D	O	E	Vi	Su	P	Fu
Hassna Agoumi	✓	✓	✓	✓	✓	✓		✓	✓	✓	✓			
Seddik Bri	✓	✓		✓	✓		✓			✓		✓		
Youssef El Amraoui	✓			✓	✓				✓			✓	✓	
Adil Saadi	✓	✓		✓						✓		✓		

C : **C**onceptualization
M : **M**ethodology
So : **So**ftware
Va : **Va**lidation
Fo : **Fo**rmal analysis
I : **I**nvestigation
R : **R**esources
D : **D**ata Curation
O : Writing - **O**riginal Draft
E : Writing - Review & **E**diting
Vi : **Vi**sualization
Su : **Su**pervision
P : **P**roject administration
Fu : **Fu**nding acquisition

CONFLICT OF INTEREST STATEMENT

The authors declare that they have no conflict of interest.

DATA AVAILABILITY

The authors confirm that the data supporting the findings of this study are available within the article.

REFERENCES

[1] G. Suguna, A. Rajesh, and K. Abirami, “Design of Compact Dual-Band 6G Antenna for Internet of Vehicles in FR3 Applications,” *Signals and Communication Technology*, vol. Part F626, pp. 435–445, 2025, doi: 10.1007/978-3-031-78802-4_27.
[2] A. Kumar, S. C. Yadav, V. Sivavenkateswara Rao, and S. P. Duttagupta, “High-gain H-plane SIW horn antenna loaded with dielectric slab for ku band low RCS applications,” *Physica Scripta*, vol. 99, no. 8, 2024, doi: 10.1088/1402-4896/ad6248.
[3] A. El Ansari, S. K. Khandare, and N. El Amrani El Idrissi, “Recent advances in graphene-based terahertz microstrip antennas: A technical review of substrate choices and emerging challenges,” *Optik*, vol. 338, 2025, doi: 10.1016/j.ijleo.2025.172507.
[4] E. García, A. Andújar, and J. Anguera, “Overview of Reconfigurable Antenna Systems for IoT Devices,” *Electronics (Switzerland)*, vol. 13, no. 20, 2024, doi: 10.3390/electronics13203988.

[5] J. Xu, C. J. Guo, and J. Ding, “Dielectric resonator used as radome and antenna: A new concept for large frequency ratio shared aperture antenna design,” *Microwave and Optical Technology Letters*, vol. 64, no. 1, pp. 174–178, 2022, doi: 10.1002/mop.33079.

[6] Y. Wang, Z. Liu, H. Zhou, J. Bornemann, Y. Wang, and X. Kong, “A High-Gain Wideband Fabry-Pérot Antenna Employing a Water-Based Frequency Selective Surface for Polarization- and RCS-Reconfigurability,” *International Journal of RF and Microwave Computer-Aided Engineering*, vol. 2024, pp. 1–12, Jan. 2024, doi: 10.1155/2024/1804375.

[7] T. Lou, X. X. Yang, G. Tan, and S. Gao, “Shared Aperture Dual-Band Dual Circularly Polarized Multibeam Antenna for Satellite-Assisted Internet of Vehicles,” *IEEE Internet of Things Journal*, vol. 11, no. 7, pp. 12000–12011, 2024, doi: 10.1109/JIOT.2023.3332092.

[8] M. Simone *et al.*, “A Low-Profile Shared Aperture Antenna for FR1 and FR2 5G Frequency Bands,” *IEEE Access*, vol. 12, pp. 71617–71627, 2024, doi: 10.1109/ACCESS.2024.3400671.

[9] Y. Bi, Y. Li, H. Wong, B. Xiao, L. Ge, and J. Wang, “A Millimeter-Wave Wideband Antenna Module With Switchable Fan-Beam Radiation for Wide Coverage of 5G IoT Applications,” *IEEE Internet of Things Journal*, vol. 10, no. 23, pp. 20969–20983, 2023, doi: 10.1109/JIOT.2023.3284848.

[10] M. Chang *et al.*, “Dual-Band Shared-Aperture Reflective Surface Featuring Wide Band-Ratio Across Sub-6 GHz and Millimeter-Wave on a Single-Layer,” *IEEE Transactions on Antennas and Propagation*, vol. 73, no. 1, pp. 665–670, 2025, doi: 10.1109/TAP.2024.3503755.

[11] Q. Chen, Y. F. Cheng, C. Liao, and X. Zhong, “Triple-band shared-aperture antenna integrating Fabry–Pérot radiator and microstrip grid array for millimeter-wave communication applications,” *AEU - International Journal of Electronics and Communications*, vol. 200, 2025, doi: 10.1016/j.aeue.2025.155866.

[12] Y. Huang *et al.*, “A Low-Profile Dual-Polarized High-Gain Low Cross-Polarization Phased Array for Ku-Band Satellite Communications,” *Sensors*, vol. 25, no. 13, 2025, doi: 10.3390/s25133986.

[13] Z. L. Ma and Y. L. Geng, “A S/K/Ka Triple-Band Shared-Aperture Antenna Hybridizing Monopole Array and Transmitarray,” *IEEE Open Journal of Antennas and Propagation*, vol. 6, no. 6, pp. 2040–2049, 2025, doi: 10.1109/OJAP.2025.3615846.

[14] B. Kalra, S. Mukherjee, G. Singh, and M. M. Sharma, “A compact dual band circularly polarized antenna using shared aperture technique for NavIC receiver,” *Sadhana - Academy Proceedings in Engineering Sciences*, vol. 50, no. 2, 2025, doi: 10.1007/s12046-025-02716-y.

[15] A. Kumar, M. Aljaidi, I. Kansal, K. Alshammari, G. Gupta, and S. M. Alenezi, “Recent Trends in Reconfigurable Antennas for Modern Wireless Communication: A Comprehensive Review,” *International Journal of Antennas and Propagation*, vol. 2024, 2024, doi: 10.1155/ijap/8816812.

[16] P.-C. Ángel, P.-E. Mario, M. Carlos, P. Pablo, G.-V. María, and G. Raphaël, “Broadband 1-bit Reconfigurable Intelligent Surface at Millimeter Waves: Overcoming PIN-Diode Degradation with Slotline Ring Topology,” *IEEE Transactions on Antennas and Propagation*, no. 62, 2025, doi: 10.1109/TAP.2025.3558424.

[17] A. Maiti and S. Mandal, “Surface Fitting Based Modelling of a Circular Microstrip Patch Antenna Operating at 3 GHz Frequency,” *International Journal of Wireless and Microwave Technologies*, vol. 14, no. 2, pp. 65–74, 2024, doi: 10.5815/ijwmt.2024.02.05.

[18] H. M. Marhoon and N. Qasem, “Simulation and optimization of tuneable microstrip patch antenna for fifth-generation applications based on graphene,” *International Journal of Electrical and Computer Engineering*, vol. 10, no. 5, pp. 5546–5558, 2020, doi: 10.11591/IJECE.V10I5.PP5546-5558.

[19] C. Y. Wei, H. C. Zhang, L. Xiao, and T. J. Cui, “Adaptive Reduction of Mutual Coupling Between Compact Frequency-Reconfigurable Antennas Using Tunable Slow-Wave Structures,” *IEEE Antennas and Wireless Propagation Letters*, vol. 24, no. 7, pp. 1699–1703, 2025, doi: 10.1109/LAWP.2025.3545421.

[20] P. Wu, Y.-H. Liu, Z.-Q. Zhao, and Q.-H. Liu, “Sparse antenna array design methodologies: A review,” *Journal of Electronic Science and Technology*, vol. 22, no. 3, Sep. 2024, doi: 10.1016/j.jnlest.2024.100276.

[21] M. A. Haque *et al.*, “Graphene based terahertz MIMO antenna with machine learning regression for 6G communications,” *Scientific Reports*, vol. 16, no. 1, p. 3900, Jan. 2026, doi: 10.1038/s41598-025-32487-9.

[22] H. J. Hwang, S. Y. Kim, S. K. Lee, and B. H. Lee, “Reconfigurable Single-Layer Graphene Radio Frequency Antenna Device Capable of Changing Resonant Frequency,” *Nanomaterials*, vol. 13, no. 7, 2023, doi: 10.3390/nano13071203.

[23] M. Al-Tamimi and R. Hamdan Thaher, “Design of New Compound Reconfigurable Microstrip Antenna for C and Ku Bands Applications,” *Journal of Engineering and Sustainable Development*, vol. 27, no. 2, pp. 196–203, Mar. 2023, doi: 10.31272/jeasd.27.2.4.

[24] S. E. Bayer Keskin, S. Koziel, and S. Szczepanski, “Frequency reconfigurable PIN diode-based Reuleaux-triangle-shaped monopole antenna for UWB/Ku band applications,” *Scientific Reports*, vol. 15, no. 1, 2025, doi: 10.1038/s41598-025-91108-7.

[25] O. H. Karabey, “Design and analysis of a continuously linear polarization agile antenna using microwave liquid crystal technology,” *Engineering Science and Technology, an International Journal*, vol. 71, 2025, doi: 10.1016/j.jestch.2025.102201.

[26] R. J. Yanti, A. I. Wahdiyat, E. T. Rahardjo, F. Y. Zulkifli, and C. Apriono, “Design of a circular patch sub-array microstrip antenna with dual linear polarization for Ku-band satellite communication applications,” *e-Prime - Advances in Electrical Engineering, Electronics and Energy*, vol. 11, 2025, doi: 10.1016/j.prime.2025.100939.

[27] I. H. Nejdi *et al.*, “A Low-Profile UWB Monopole Antenna and High-Isolated UWB-MIMO Antenna for Wireless Communications Networks,” *Progress in Electromagnetics Research C*, vol. 161, pp. 105–119, 2025, doi: 10.2528/PIERC25082106.

[28] Shailesh, G. Srivastava, S. Kumar, D. Sharma, B. Goyal, and N. F. Soliman, “A common grounded ultra-wideband diversity/MIMO antenna with high inter-element isolation,” *Scientific Reports*, vol. 15, no. 1, 2025, doi: 10.1038/s41598-025-10635-5.

[29] S. Trinh-Van, W. Y. Yang, H. W. Cho, and K. C. Hwang, “A Four-Port Dual-Band Dual-Polarized Antenna for Ku-Band Satellite Communications,” *Applied Sciences (Switzerland)*, vol. 14, no. 7, 2024, doi: 10.3390/app14072730.

[30] A. A. Ibrahim and M. F. Abo Sree, “UWB MIMO antenna with 4-element, compact size, high isolation and single band rejection for high-speed wireless networks,” *Wireless Networks*, vol. 28, no. 7, pp. 3143–3155, 2022, doi: 10.1007/s11276-022-03019-4.

BIOGRAPHIES OF AUTHORS

Hassna Agoumi received her Master's degree in Telecommunications and Microwave Devices from Sidi Mohamed Ben Abdellah University, Fes, Morocco, in 2011 and her Bachelor's degree in Electrical Engineering from Moulay Ismail University, Meknes, Morocco, in 2005. She is currently a Ph.D. student in Electrical Engineering at Moulay Ismail University, Meknes, Morocco. She can be contacted at email: h.agoumi@edu.umi.ac.ma.

Seddik Bri is a Professor at the High School of Technology (ESTM), Moulay Ismail University, Meknes, Morocco. His research interests include material characterization, patch antenna design, microwave applications, and security in communication systems. He has contributed to several studies on antenna design and microwave devices. He can be contacted at email: s.bri@umi.ac.ma.

Youssef El Amraoui received his Bachelor's and Master's degrees in Physics from Mohammed V University, Rabat, Morocco, in 1989 and 1990, respectively, and his Ph.D. in Physics from Moulay Ismail University, Meknes, Morocco, in 1998. He is currently a Professor at Mohammed V University, Rabat, Morocco. His research focuses on the theoretical study of phase transitions in disordered systems. He can be contacted at email: yelamraoui@hotmail.com.

Adil Saadi was born in Morocco in 1970. He received his Ph.D. from Ibn Tofail University, Kenitra, Morocco, in 2003. He is currently a Professor at Moulay Ismail University, Meknes, Morocco. His research interests include microwave biomedical applications such as hyperthermia and cancer detection. He is currently developing microwave components using transverse section method or TSM for industrial microwave applications. He can be contacted at email: a.saadi@umi.ac.ma.